

# Cross-sections and analyzing powers for $(p, n)$ reactions on $^3\text{He}$ and $^4\text{He}$ at 346 MeV

E. Ihara,<sup>1</sup> T. Wakasa,<sup>1,\*</sup> M. Dozono,<sup>1</sup> K. Hatanaka,<sup>2</sup> T. Imamura,<sup>1</sup> M. Kato,<sup>2</sup> S. Kuroita,<sup>1</sup>  
H. Matsubara,<sup>2</sup> T. Noro,<sup>1</sup> H. Okamura,<sup>2</sup> K. Sagara,<sup>1</sup> Y. Sakemi,<sup>3</sup> K. Sekiguchi,<sup>4</sup>  
K. Suda,<sup>4</sup> T. Sueta,<sup>1</sup> Y. Tameshige,<sup>2</sup> A. Tamii,<sup>2</sup> H. Tanabe,<sup>1</sup> and Y. Yamada<sup>1</sup>

<sup>1</sup>*Department of Physics, Kyushu University, Higashi, Fukuoka 812-8581, Japan*

<sup>2</sup>*Research Center for Nuclear Physics,*

*Osaka University, Ibaraki, Osaka 567-0047, Japan*

<sup>3</sup>*Cyclotron and Radioisotope Center,*

*Tohoku University, Sendai, Miyagi 980-8578, Japan*

<sup>4</sup>*RIKEN Nishina Center, Wako, Saitama 351-0198, Japan*

(Dated: July 9, 2008)

## Abstract

The cross-sections and analyzing powers for  $(p, n)$  reactions on  $^3\text{He}$  and  $^4\text{He}$  have been measured at a bombarding energy of  $T_p = 346$  MeV and reaction angles of  $\theta_{\text{lab}} = 9.4^\circ\text{--}27^\circ$ . The energy transfer spectra for  $^3\text{He}(p, n)$  at large  $\theta_{\text{lab}}$  ( $\geq 16^\circ$ ) are dominated by quasielastic contributions, and can be reasonably reproduced by plane-wave impulse approximation (PWIA) calculations for quasielastic scattering. By contrast, the known  $L = 1$  resonances in  $^4\text{Li}$  are clearly observed near the threshold in the  $^4\text{He}(p, n)$  spectra. Because these contributions are remarkable at small angles, the energy spectra are significantly different from those expected for quasielastic scattering. The data are compared with the PWIA calculations, and it is found that the quasielastic contributions are dominant at large  $\theta_{\text{lab}}$  ( $\geq 22^\circ$ ). The nuclear correlation effects on the quasielastic peak for  $^4\text{He}(p, n)$  are also discussed.

PACS numbers: 25.40.Kv, 24.70.+s, 25.10.+s, 27.10.+h

---

\*wakasa@phys.kyushu-u.ac.jp; <http://www.kutl.kyushu-u.ac.jp/~wakasa>

## I. INTRODUCTION

In this article, we present the cross-sections and analyzing powers for  $(p, n)$  reactions on  $^3\text{He}$  and  $^4\text{He}$  at a proton incident energy of  $T_p = 346$  MeV and laboratory reaction angles of  $\theta_{\text{lab}} = 9.4^\circ\text{--}27^\circ$ . The quasielastic scattering data obtained at  $T_p = 346$  MeV is of particular interest since the experimental data including the present results can cover a wide range of nuclei from  $^2\text{H}$  to  $^{208}\text{Pb}$  at the same incident energy [1, 2, 3]. It should be noted that the distortion in the nuclear mean field is minimal for a nucleon kinetic energy of about 300 MeV. Thus, the experimental data will provide important information to test theoretical calculations for the quasielastic process.

One of the unique features of the  $(p, n)$  quasielastic reaction is that the observed peak of the quasielastic distribution is shifted at higher excitation energy of about 20 MeV than expected from free nucleon-nucleon ( $NN$ ) kinematics [4]. Discrepancies between experimental data and theoretical predictions based on the free  $NN$  interaction may arise, for example, from nuclear many-body effects [5] or multi-step effects [6]. For the  $^2\text{H}(p, n)$  reaction, the peak position is consistent with the corresponding free  $NN$  value, and the quasielastic distribution is reasonably reproduced by plane-wave impulse approximation (PWIA) calculations [2]. The multi-step effects for  $A \leq 4$  nuclei are expected to be much smaller than those for medium and heavy nuclei. Thus the data for  $A \leq 4$  systems give clear information on the nuclear many-body effects including nuclear correlations. Hence it is very interesting to investigate whether the  $^3\text{He}(p, n)$  data can be reproduced with first-order model calculations.

In contrast to the  $^3\text{He}(p, n)$  reaction, the spectra of the  $^4\text{He}(p, n)$  reaction exhibit prominent resonances with angular momentum transfer  $L = 1$  near the threshold [7]. In the measurements at  $T_p = 100$  and 200 MeV [8, 9, 10], there is no distinct quasielastic peak in the measured spectra because the resonance contributions are dominant. These data have been compared with calculations obtained using the quasielastic scattering code THREEDEE [9] and with recoil-corrected continuum shell-model (RCCSM) calculations [8, 10]. Both calculations reproduce the  $L = 1$  resonance contributions qualitatively, however, quantitative reproduction could not be achieved for the  $L = 1$  resonance or quasielastic contributions.

The present data are compared with the calculations for quasielastic scattering [5], which have been used extensively to analyze quasielastic scattering data measured at LAMPF [11, 12, 13] and RCNP [1, 3]. The  $^3\text{He}(p, n)$  data at large angles are reasonably reproduced

by the PWIA calculations, which certify the predominance of the quasielastic process around the peak region and the weakness of the nuclear correlations. The calculations slightly underestimate the cross-sections at small angles, which might be due to the proposed isospin  $T = 3/2$  three-nucleon resonance [14, 15]. For  ${}^4\text{He}(p, n)$ , the underestimation is significant at small angles because the  $L = 1$  resonances in  ${}^4\text{Li}$  could not be described in the present quasielastic formalism. At large angles, where the quasielastic process is dominant, a significant difference is observed between the experimental and theoretical results for the peak positions. The large  $Q$ -value and nuclear correlation effects are investigated since these effects are expected to be important in  ${}^4\text{He}$  [16]. It is found that the discrepancy could be resolved in part by the nuclear correlations.

## II. EXPERIMENTAL METHODS

The experiment was carried out using the West-South Beam Line (WS-BL) [17] at the Research Center for Nuclear Physics (RCNP), Osaka University. The beam line configuration and the doubly achromatic beam properties have been reported previously [17]. In the following, therefore, we discuss experimental details relevant to the present experiment.

### A. Polarized proton beam

The polarized proton beam was produced by the high-intensity polarized ion source (HIPIS) at RCNP [18]. In order to minimize geometrical false asymmetries, the nuclear polarization state was cycled every 5 s between the normal and reverse states (e.g., between the “up” and “down” states at the target position) by selecting rf transitions. The beam was accelerated to  $T_p = 346$  MeV by using the AVF and ring cyclotrons. One out of seven beam pulses was selected before injecting into the Ring cyclotron. This pulse selection yielded a beam pulse period of 431 ns, and reduced the wraparound of slow neutrons from preceding beam pulses. A single-turn extraction was maintained during the measurement in order to keep the beam pulse period. Multi-turn extracted protons were less than 1% of single-turn extracted protons.

The beam polarization was continuously monitored with the beam-line polarimeter BLP1 [17]. The polarimeter consisted of four pairs of conjugate-angle plastic scintillators. The

$\vec{p} + p$  elastic scattering was used as the analyzing reaction, and the elastically scattered and recoiled protons were detected in kinematical coincidence with a pair of scintillators. A self-supporting  $\text{CH}_2$  target with a thickness of  $1.1 \text{ mg/cm}^2$  was used as the hydrogen target. The typical magnitude of the beam polarization was about 0.52.

### B. $^3\text{He}$ and $^4\text{He}$ targets

The  $^3\text{He}$  and  $^4\text{He}$  targets were prepared as high-pressure cooled gas targets [15] by using a target system developed for a liquid  $\text{H}_2$  target [19]. This target was operated at temperatures down to 29 K and at absolute pressures up to 2.5 atm. Both the cell temperature and pressure were continuously monitored during the experiment, and the typical target densities were about  $1.2 \times 10^{21} \text{ cm}^{-2}$  and  $1.0 \times 10^{21} \text{ cm}^{-2}$  for  $^3\text{He}$  and  $^4\text{He}$ , respectively. The gas cell windows were made of 12- $\mu\text{m}$ -thick Alamid foil. Background spectra were also measured by filling the target cell with  $\text{H}_2$  gas in order to subtract the contributions from both the Alamid windows and the beam ducts. We also measured data with  $\text{D}_2$  gas in the target cell to determine the detection efficiency of the neutron detector system. These data were also used to estimate the systematic uncertainty as described below because the cross-sections are reliably predicted by the theoretical calculations.

### C. Dipole magnet and neutron detector

A dipole magnet made of permanent NEOMAX magnets [20] was installed 10 cm downstream from the target. This magnet had a magnetic rigidity of  $B\rho = 0.95 \text{ Tm}$ , which was sufficient to sweep charged particles from the target in order to prevent them from entering the neutron detector system.

Neutrons were measured with a 20 m flight path length at  $\theta_{\text{lab}} = 9.4^\circ\text{--}27^\circ$ . As illustrated in Fig. 1, the neutron detector system consisted of 20 sets of one-dimensional position-sensitive plastic scintillators (BC408) with a size of  $100 \times 10 \times 5 \text{ cm}^3$ , which was part of the NPOL3 system [21]. The detector system consisted of four planes of neutron detectors, each with an effective solid angle of  $\Delta\Omega = 1.25 \text{ msr}$ .

### III. DATA REDUCTION

#### A. Background subtraction

The neutrons from the target windows are the dominant source of the background at lower energy transfers of  $\omega_{\text{lab}} \lesssim 50$  MeV. This contribution can be subtracted by measuring the empty-target spectra. However, the background from the beam ducts downstream from the target becomes significant at higher energy transfers. The proton beam was spread out by the multiple scattering in the target material, and part of it hit the beam ducts. This contribution depends on the target density, and thus we could not subtract it with the empty-target spectra. Thus, we also measured the data with  $\text{H}_2$  gas in the target cell because the multiple scattering effects for He and  $\text{H}_2$  are expected to be similar. Figure 2 shows a representative set of spectra as a function of energy transfer. In the  $\text{H}_2 + \text{Cell}$  spectrum, a shoulder component is observed at  $\omega_{\text{lab}} \simeq 26$  MeV. This bump is mainly due to the spin-dipole resonances (SDRs) in  $^{12}\text{N}$  excited by the  $(p, n)$  reaction on  $^{12}\text{C}$  in Alamid. The yield at  $\omega_{\text{lab}} \gtrsim 30$  MeV consists of the quasielastic  $(p, n)$  reaction events for the Alamid windows and the background neutrons from the beam ducts.

The filled histogram in Fig. 2 shows the subtraction results. The background contributions including the SDR bump in  $^{12}\text{N}$  are successfully subtracted without adjusting the relative normalization. We have also measured the data for the  $^2\text{H}(p, n)$  reaction in order to investigate the reliability of the background subtraction. The results are discussed in the next section.

#### B. Background subtracted observables

Observables for the  $A(p, n)$  reaction ( $A$  represents  $^2\text{H}$ ,  $^3\text{He}$ , or  $^4\text{He}$ ) were extracted through a cross-section-weighted subtraction of the observables for the  $\text{H}_2$  target ( $\text{H}_2 + \text{Cell}$ ) from the observables for the  $A$  target ( $A + \text{Cell}$ ) as

$$\sigma_A = \sigma_{A+\text{Cell}} - \sigma_{\text{H}_2+\text{Cell}} , \quad (1a)$$

$$D_A = \frac{D_{A+\text{Cell}} - f D_{\text{H}_2+\text{Cell}}}{1 - f} , \quad (1b)$$

where  $\sigma$  represents the cross-section,  $D$  is the analyzing power  $A_y$ , and  $f = \sigma_{\text{H}_2+\text{Cell}}/\sigma_{A+\text{Cell}}$ . The fraction  $f$  was estimated by using the cross-sections based on the nominal target thick-

nesses and integrated beam current.

### C. Neutron detection efficiency and energy resolution

The neutron detection efficiency was determined using the  ${}^2\text{H}(p, n)$  reaction at  $\theta_{\text{lab}} = 22^\circ$  whose cross-section at  $T_p = 345$  MeV is known [2]. The result is  $0.035 \pm 0.002$ , where the uncertainty comes mainly from the uncertainty in the thickness of the  ${}^2\text{H}$  target.

The overall energy resolution was determined by measuring the  $p + p$  elastic scattering for the  $\text{H}_2$  target. The result is  $\Delta E = 7.7$  MeV in full width at half maximum.

## IV. RESULTS AND DISCUSSIONS

### A. ${}^2\text{H}(p, n)$ data

The cross-sections and analyzing powers for the  ${}^2\text{H}(p, n)$  reaction at  $T_p = 346$  MeV and  $\theta_{\text{lab}} = 9.4^\circ - 27^\circ$  are presented in Fig. 3. The cross-sections are binned in 1 MeV intervals, while the analyzing powers are binned in 5 MeV intervals. The tail components of the quasielastic distributions at the lower energy transfer side are mainly due to the  ${}^1\text{S}_0$  final state interaction (FSI) of the residual two-proton system. The peak positions  $\omega_{\text{QES}}$  of the quasielastic distributions coincide with the energy transfers of the corresponding free  $NN$  scattering indicated by the dotted vertical lines, which is consistent with the results at other incident energies [2, 12, 22].

The data have been compared with the theoretical predictions obtained through PWIA using the computer code DPN [23]. These calculations have reproduced the previous  ${}^2\text{H}(p, n)$  data at  $T_p = 345$  MeV and  $\theta_{\text{lab}} = 16^\circ, 22^\circ$ , and  $27^\circ$ , not only for the cross-sections but also for the polarization observables [2]. The previous data were measured at the neutron time-of-flight facility [24] at RCNP under a significantly low-background condition. Thus a comparison between the present data and these theoretical calculations allows us to investigate the reliability of the present background subtraction. In the calculations, the wave functions of the initial deuteron and the final  $pp$ -scattering state are generated by the Reid soft core potential. Both  $S$  and  $D$  states are included in the deuteron, and the FSI process is also included in the  $pp$  scattering. The  $NN$   $t$ -matrix parameterized by Bugg and Wilkin [25, 26] is used in the impulse approximation.

The solid curves in Fig. 3 represent the corresponding calculations smeared by a resolution function with  $\Delta E = 7.7$  MeV. The calculations reproduce both the cross-sections and analyzing powers around the quasielastic peak reasonably well, but underpredict the data beyond the quasielastic peak. Because these calculations have reasonably reproduced the previous  ${}^2\text{H}(p, n)$  data within about 10% in the present energy transfer region [2], the systematic uncertainty of the present data around the quasielastic peak ( $\omega_{\text{lab}} \lesssim \omega_{\text{QES}} + 20$  MeV) is estimated to be about 10%, whereas that beyond the quasielastic peak would be much larger. Thus, in the following discussions, we focus on the comparison between experimental and theoretical results around the quasielastic peak.

### B. ${}^3\text{He}(p, n)$ data

Figure 4 shows the cross-sections and analyzing powers for the  ${}^3\text{He}(p, n)$  reaction at  $T_p = 346$  MeV and  $\theta_{\text{lab}} = 9.4^\circ$ – $27^\circ$ . The analyzing power data for  ${}^2\text{H}(p, n)$  are also shown by the open squares. The vertical dashed lines represent the energy transfers  $\omega_{NN}$  for the free  $NN$  scattering. The analyzing powers for  ${}^3\text{He}(p, n)$  are in reasonable agreement with those for  ${}^2\text{H}(p, n)$ . Thus, the quasielastic process is expected to be dominant for  ${}^3\text{He}(p, n)$  as well. However, the peak position of the cross-sections is significantly higher than the energy transfer for the corresponding free  $NN$  scattering. The  $Q$ -value and Pauli principle effects are expected to be more significant than those for  ${}^2\text{H}(p, n)$ . Therefore, in the following, we perform PWIA calculations in order to investigate these effects quantitatively.

### C. PWIA calculations for ${}^3\text{He}(p, n)$

We performed the PWIA calculations by using the computer code CRDW [5]. The formalism for the response function is that of Nishida and Ichimura [27], and the free response function is employed in the present calculations. The single-particle wave functions were generated by a Woods-Saxon (WS) potential. The radial and diffuseness parameters were determined to be  $r_0 = 0.92$  fm and  $a_0 = 0.38$  fm, respectively, to reproduce the density distribution of  ${}^3\text{He}$  [28]. The depth of the WS potential was adjusted to reproduce the separation energy of the  $0s_{1/2}$  orbit. The optimal factorization prescription [29, 30, 31, 32] is employed to model the Fermi motion of the target nucleons. The  $NN$   $t$ -matrix parameterized

by Bugg and Wilkin [25, 26] was used.

The solid curves in Fig. 4 represent the corresponding calculations. We focus on the energy transfer region of  $\omega_{\text{lab}} \lesssim \omega_{\text{QES}} + 20$  MeV on the basis of the discussion in Sec. IV A. The calculations reproduce the shapes of the cross-sections reasonably well, and they also reproduce the analyzing powers fairly well around the peak. The agreement between the experimental and theoretical results for the peak positions validates the treatment of the  $Q$ -value and Pauli principle effects in the calculations. However, the cross-sections at small angles are significantly underestimated around the peak. This discrepancy between the experimental and theoretical results might be due to the three-nucleon resonance with isospin  $T = 3/2$  [14, 15]. At large  $\theta_{\text{lab}} (\geq 16^\circ)$ , where the resonance contribution is expected to be small, the calculations yield good descriptions of the cross-sections around the peak. Thus, we have confirmed that the quasielastic process is dominant around the peak region and it is described in the present theoretical framework without the nuclear correlations. Therefore, in the following, we use the same framework for  ${}^4\text{He}(p, n)$  in order to investigate the nuclear correlation effects in the present data.

#### D. ${}^4\text{He}(p, n)$ data

The cross-sections and analyzing powers for the  ${}^4\text{He}(p, n)$  reaction at  $T_p = 346$  MeV and  $\theta_{\text{lab}} = 9.4^\circ$ – $27^\circ$  are displayed in Fig. 5 as a function of energy transfer. The data for the cross-sections and analyzing powers are binned in 1 and 5 MeV intervals, respectively. In contrast to the  ${}^3\text{He}(p, n)$  spectra, there is a steep rise near the threshold at all reaction angles. For small  $\theta_{\text{lab}} (\leq 16^\circ)$ , the transitions to the ground state with  $J^\pi = 2^-$  and the first excited state with  $J^\pi = 1^-$  of  ${}^4\text{Li}$  form a bump near the threshold. This bump is prominent compared with the data at  $T_p = 100$  MeV [10] because these spin-flip transitions are predominantly excited at projectile energies around 300 MeV. The vertical dashed lines represent the energy transfers  $\omega_{NN}$  for the free  $NN$  scattering. For large  $\theta_{\text{lab}} (\geq 22^\circ)$ , where the resonance contributions are expected to be small, the peak position of the cross-sections is significantly higher than the corresponding  $\omega_{NN}$  because of both the large  $Q$ -value and nuclear correlation effects. In the following, we compare our data with the theoretical calculations by employing these effects consistently.



### E. PWIA calculations for ${}^4\text{He}(p, n)$

The formalism of the calculations is the same as that used for  ${}^3\text{He}(p, n)$ . The nuclear mean field is described by the WS potential, and its radial and diffuseness parameters were determined to be  $r_0 = 0.83$  fm and  $a_0 = 0.33$  fm, respectively, to reproduce the density distribution of  ${}^4\text{He}$  [28]. The results are shown as solid curves in Fig. 5. The calculations significantly underestimate the cross-sections around the peak at small angles. This discrepancy is mainly due to the  $L = 1$  resonance contributions near the threshold, which are not described by the simple particle-hole excitation employed in the present calculations. For the analyzing powers, the calculations systematically yield smaller values than the experimental data, especially at small angles. This underestimation might also be due to the resonance contributions in the experimental data.

It should be noted that the observed peak positions of the cross-sections are significantly higher than the theoretical predictions at large values of  $\theta_{\text{lab}}$  ( $\theta_{\text{lab}} = 22^\circ$  and  $27^\circ$ ). Because the resonance contributions shift the cross-sections to lower energy transfer values, the discrepancy between the experimental and theoretical results might be indicative of nuclear correlation effects, which are expected to be large for  ${}^4\text{He}$  [16]. Thus we performed the PWIA calculations with the random phase approximation (RPA) response functions, employing the  $\pi + \rho + g'$  model interaction [27]. For the pion and rho-meson exchange interactions, we have used the coupling constants and meson parameters from the Bonn potential, which treats  $\Delta$  explicitly [33]. The Landau-Migdal parameters  $g'$  were estimated to be  $g'_{NN} = 0.65$  and  $g'_{N\Delta} = 0.35$  [34, 35] by using the peak position of the Gamow-Teller (GT) giant resonance and the GT quenching factor at  $q = 0$  [36, 37], as well as the isovector spin-longitudinal polarized cross-section in the QES process at  $q \simeq 1.7$  fm $^{-1}$  [3]. Here, we fixed  $g'_{\Delta\Delta} = 0.5$  [38] since the  $g'_{\Delta\Delta}$  dependence of the results is very weak. The dashed curves in Fig. 5 show the results obtained by employing the RPA response function. The nuclear correlation effects are expected to be significant in both the cross-sections and analyzing powers. We have also performed the PWIA calculations with the RPA response function for  ${}^3\text{He}(p, n)$ , however, the nuclear correlation effects were very small. The cross-sections are shifted to higher energy transfer values by considering the nuclear correlation effects, which is due to the hardening effects in the spin-transverse mode. The discrepancy of the peak positions at  $\theta_{\text{lab}} = 22^\circ$  and  $27^\circ$  is resolved in part by considering the nuclear correlation

effects. However, it is difficult to conclude whether the nuclear correlations are observed in the present data because the resonance contributions, which are important for quantitative description especially at small angles, are not included in the present calculations. Thus detailed theoretical investigations including both the resonance and nuclear correlation effects are required.

## V. SUMMARY AND CONCLUSION

We have measured the cross-sections and analyzing powers for  $(p, n)$  reactions on  $^3\text{He}$  and  $^4\text{He}$  at  $T_p = 346$  MeV and  $\theta_{\text{lab}} = 9.4^\circ\text{--}27^\circ$ . Both data are compared with the PWIA calculations for quasielastic scattering. The calculations can reproduce the  $^3\text{He}(p, n)$  data at large  $\theta_{\text{lab}}$  values ( $\geq 16^\circ$ ) reasonably well. At small  $\theta_{\text{lab}}$  values ( $\leq 13^\circ$ ), the observed cross-sections are slightly larger than the calculations, which might suggest the contribution from the  $T = 3/2$  three-nucleon resonance. In contrast to the  $^3\text{He}(p, n)$  reaction,  $L = 1$  resonance contributions are clearly observed near the threshold for the  $^4\text{He}(p, n)$  reaction. At large  $\theta_{\text{lab}}$  values ( $\geq 22^\circ$ ), where the resonance contributions are small, the PWIA calculations yield reasonable descriptions for the cross-sections, whereas the peak positions are significantly lower than the experimental values. The observed peak shift can be explained in part by considering the nuclear correlations. However, the present data are not conclusive evidence for the nuclear correlation effects, and call for theoretical calculations that incorporate the proper description for the  $L = 1$  resonances in order to settle the interpretation of the present data.

## Acknowledgments

We are grateful to Professor M. Ichimura for his helpful correspondence. We also acknowledge the dedicated efforts of the RCNP cyclotron crew for providing a high quality polarized proton beam. The experiment was performed at RCNP under Program Number E300. This research was supported in part by the Ministry of Education, Culture, Sports, Science, and Technology of Japan.

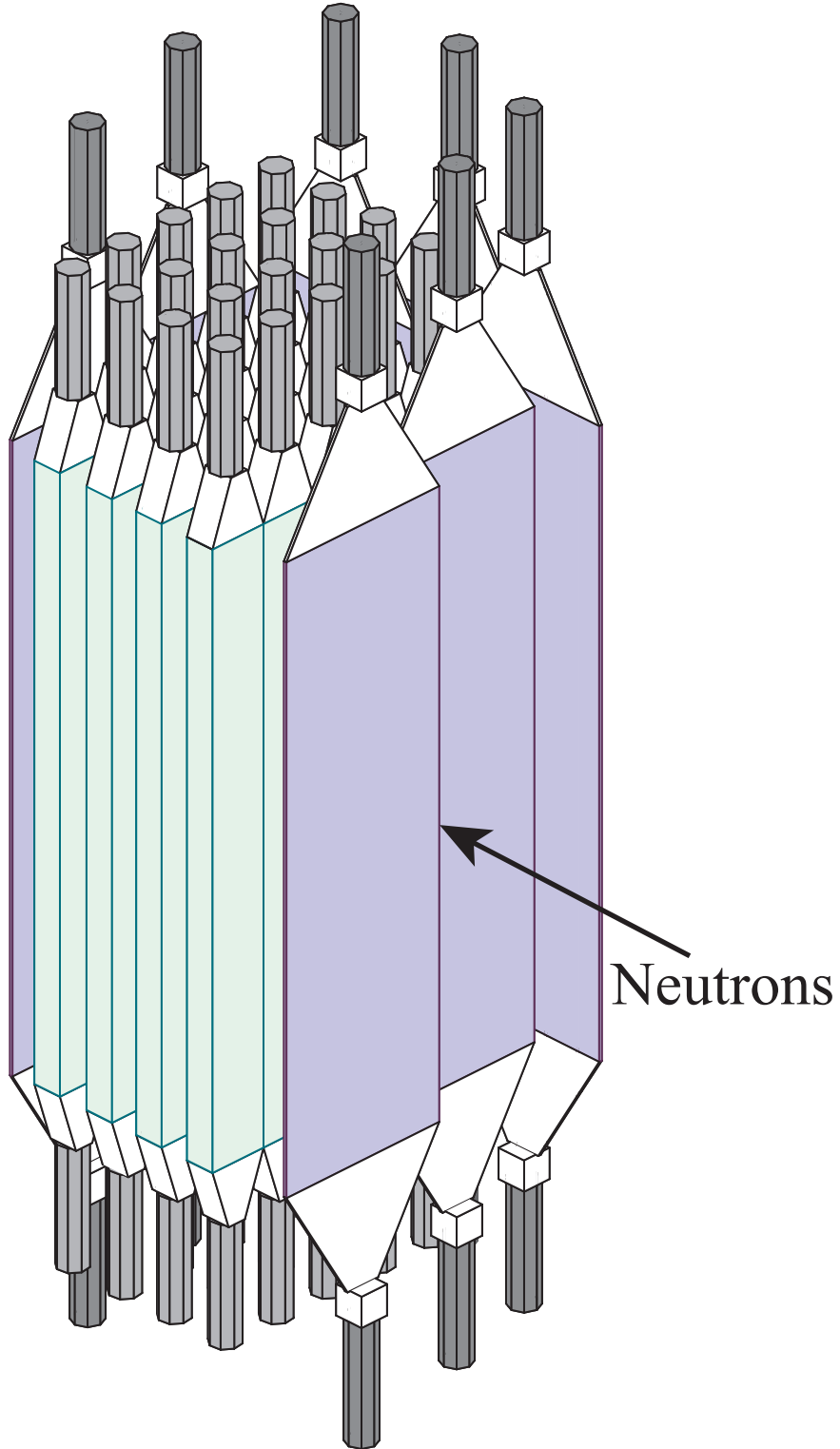


FIG. 1: (Color online) A schematic view of the neutron detector system. The 20 sets of neutron detectors are surrounded by thin plastic scintillation detectors in order to reject charged particles.

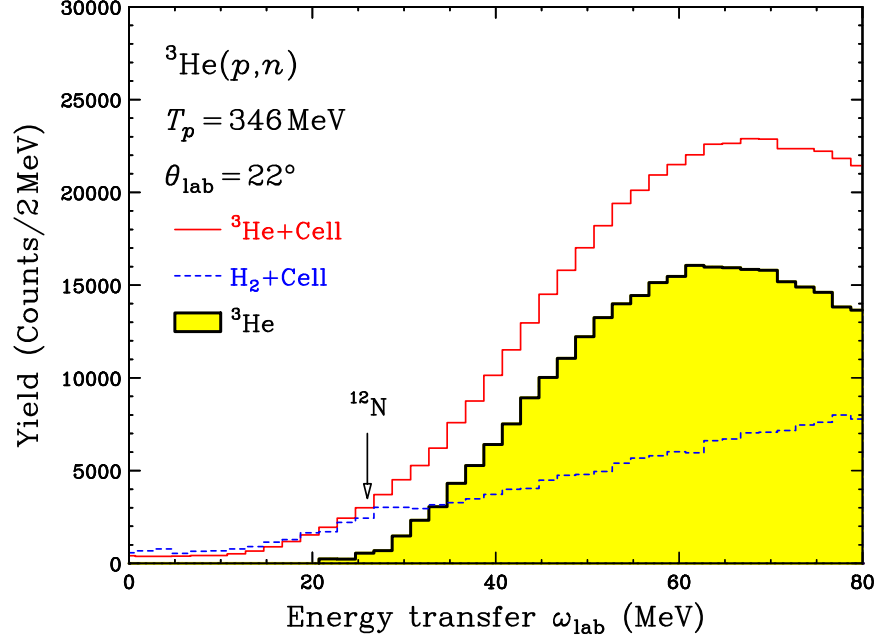


FIG. 2: (Color online) Energy transfer spectra for the targets filled with  ${}^3\text{He}$  (thin solid histogram) and  $\text{H}_2$  (dash histogram) gases for the  $(p,n)$  reaction at  $T_p = 346 \text{ MeV}$  and  $\theta_{\text{lab}} = 22^\circ$ . The filled thick solid histogram shows the spectrum for the  ${}^3\text{He}(p,n)$  reaction obtained by the subtraction.

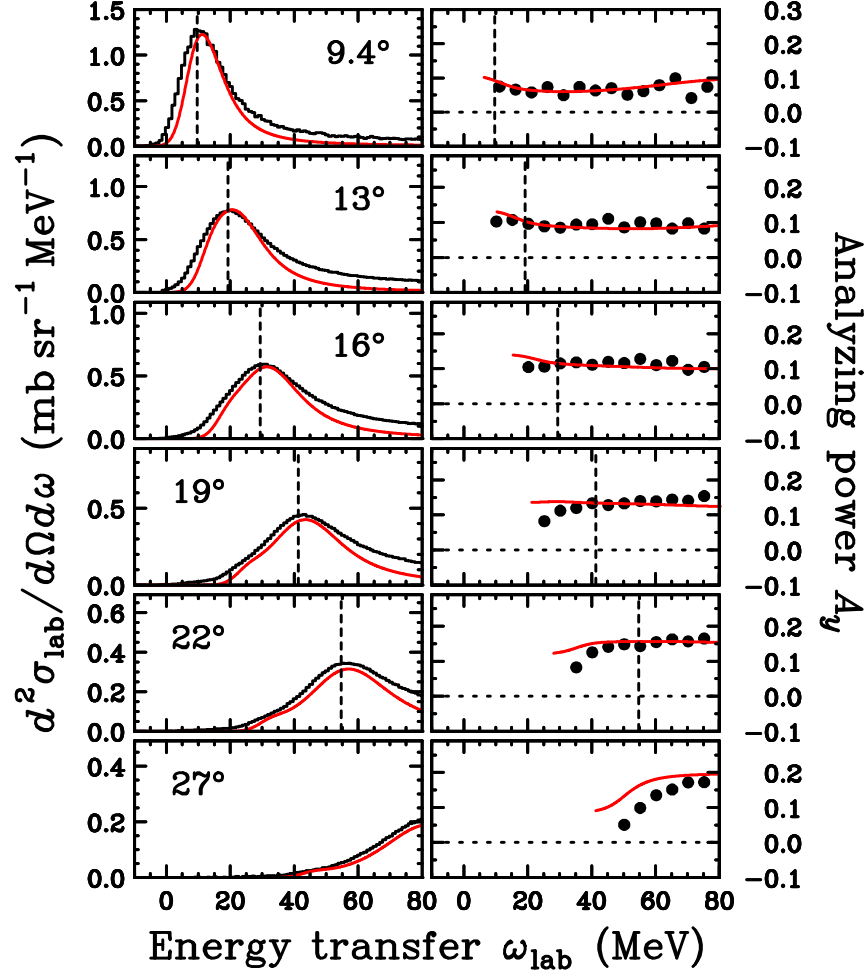


FIG. 3: (Color online) The cross-sections (left panels) and analyzing powers (right panels) for the  $^2\text{H}(p,n)$  reaction at  $T_p = 346$  MeV and  $\theta_{\text{lab}} = 9.4^\circ$ – $27^\circ$ . The vertical dashed lines represent the energy transfers for the free  $NN$  scattering. The solid curves are the PWIA predictions obtained by the optimal factorization approximation.

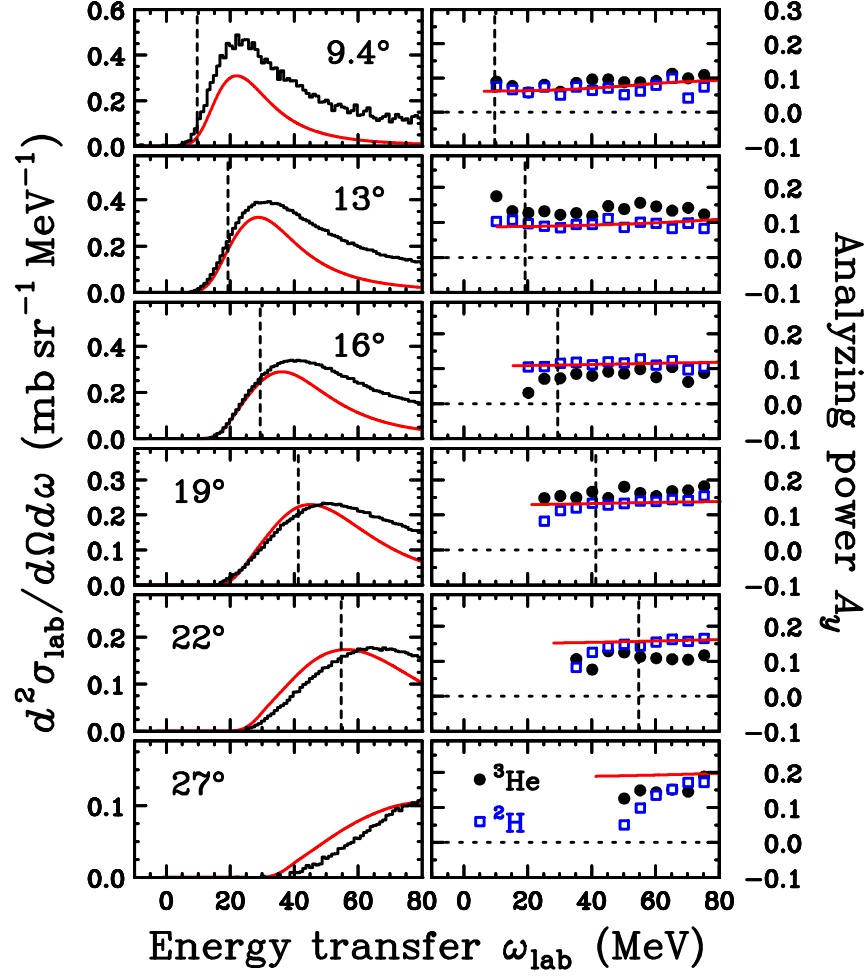


FIG. 4: (Color online) The cross-sections (left panels) and analyzing powers (right panels) for the  $^3\text{He}(p, n)$  reaction at  $T_p = 346$  MeV and  $\theta_{\text{lab}} = 9.4^\circ$ – $27^\circ$ . The analyzing power data for  $^2\text{H}(p, n)$  are also shown by the open squares. The vertical dashed lines represent the energy transfers for the free  $NN$  scattering. The solid curves represent the PWIA calculations.

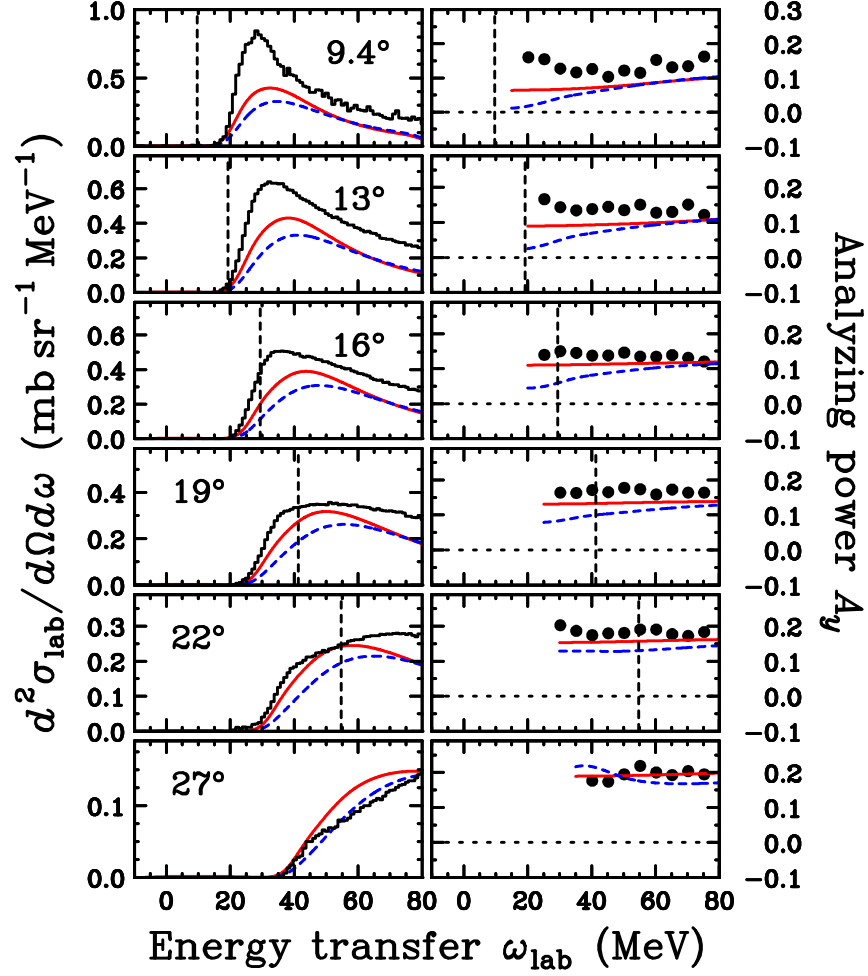


FIG. 5: (Color online) The cross-sections (left panels) and analyzing powers (right panels) for the  ${}^4\text{He}(p, n)$  reaction at  $T_p = 346$  MeV and  $\theta_{\text{lab}} = 9.4^\circ$ – $27^\circ$ . The vertical dashed lines represent the energy transfers for the free  $NN$  scattering. The solid and dashed curves represent the PWIA calculations performed using free and RPA response functions, respectively.

- 
- [1] T. Wakasa et al., Phys. Rev. C **59**, 3177 (1999).
  - [2] T. Wakasa et al., Phys. Rev. C **69**, 044602 (2004).
  - [3] T. Wakasa et al., Phys. Rev. C **69**, 054609 (2004).
  - [4] D. L. Prout et al., Phys. Rev. C **52**, 228 (1995).
  - [5] K. Kawahigashi, K. Nishida, A. Itabashi, and M. Ichimura, Phys. Rev. C **63**, 044609 (2001).
  - [6] Y. Nakaoka, Phys. Rev. C **65**, 064616 (2002).
  - [7] D. R. Tilley, H. R. Weller, and G. M. Hale, Nucl. Phys. A **541**, 1 (1992).
  - [8] C. M. Edwards et al., Phys. Lett. B **368**, 39 (1996).
  - [9] M. Palarczyk et al., Phys. Rev. C **58**, 645 (1998).
  - [10] C. M. Riedel et al., Phys. Rev. C **69**, 024616 (2004).
  - [11] J. B. McClelland et al., Phys. Rev. Lett. **69**, 582 (1992).
  - [12] X. Y. Chen et al., Phys. Rev. C **47**, 2159 (1993).
  - [13] T. N. Taddeucci et al., Phys. Rev. Lett. **73**, 3516 (1994).
  - [14] L. E. Williams, C. J. Batty, B. E. Bonner, C. Tschalär, H. C. Benöhr, and A. S. Clouth, Phys. Rev. Lett. **23**, 1181 (1969).
  - [15] T. Wakasa et al., Phys. Rev. C **77**, 054611 (2008).
  - [16] V. R. Pandharipande, J. Carlson, S. C. Pieper, R. B. Wiringa, and R. Schiavilla, Phys. Rev. C **49**, 789 (1994).
  - [17] T. Wakasa et al., Nucl. Instrum. Methods Phys. Res. A **482**, 79 (2002).
  - [18] K. Hatanaka, K. Takahisa, H. Tamura, M. Sato, and I. Miura, Nucl. Instrum. Methods Phys. Res. A **384**, 575 (1997).
  - [19] T. Yagita et al., Mod. Phys. Lett. A **18**, 322 (2003).
  - [20] <http://www.hitachi-m-admet.com/>.
  - [21] T. Wakasa et al., Nucl. Instrum. Methods Phys. Res. A **547**, 569 (2005).
  - [22] D. L. Prout et al., Phys. Rev. C **65**, 034611 (2002).
  - [23] A. Itabashi, K. Aizawa, and M. Ichimura, Prog. Theor. Phys. **91**, 69 (1994).
  - [24] H. Sakai, H. Okamura, H. Otsu, T. Wakasa, S. Ishida, N. Sakamoto, T. Uesaka, Y. Satou, S. Fujita, and K. Hatanaka, Nucl. Instrum. Methods Phys. Res. A **369**, 120 (1996).
  - [25] D. V. Bugg and C. Wilkin, Phys. Lett. B **152**, 37 (1985).



- [26] D. V. Bugg and C. Wilkin, Nucl. Phys. A **467**, 575 (1987).
- [27] K. Nishida and M. Ichimura, Phys. Rev. C **51**, 269 (1995).
- [28] C. W. de Jager, H. de Vries, and C. de Vries, At. Data Nucl. Data Tables **14**, 479 (1974).
- [29] A. Picklesimer, P. C. Tandy, R. M. Thaler, and D. H. Wolfe, Phys. Rev. C **30**, 1861 (1984).
- [30] S. A. Gurvitz, Phys. Rev. C **33**, 422 (1986).
- [31] X. Q. Zhu, N. Mobed, and S. S. M. Wong, Nucl. Phys. A **466**, 623 (1987).
- [32] M. Ichimura and K. Kawahigashi, Phys. Rev. C **45**, 1822 (1992).
- [33] R. Machleidt, K. Holinde, and C. Elster, Phys. Rep. **149**, 1 (1987).
- [34] T. Wakasa, M. Ichimura, and H. Sakai, Phys. Rev. C **72**, 067303 (2005).
- [35] M. Ichimura, H. Sakai, and T. Wakasa, Prog. Part. Nucl. Phys. **56**, 446 (2006).
- [36] T. Wakasa et al., Phys. Rev. C **55**, 2909 (1997).
- [37] K. Yako et al., Phys. Lett. B **615**, 193 (2005).
- [38] W. H. Dickhoff et al., Phys. Rev. C **23**, 1154 (1981).